

## Micellization and Inhibition Efficiency

Yi He<sup>a</sup>, Shuai Ren<sup>a</sup>, Zineb Belarbi<sup>a</sup>, Xi Wang<sup>a</sup>, David Young<sup>a</sup>, Marc Singer<sup>a</sup>, Maalek Mohamed-Saïd<sup>b</sup>,  
Sheyla Camperos<sup>c</sup>

<sup>a</sup>Institute for Corrosion and Multiphase Technology  
Department of Chemical and Biomolecular Engineering  
Ohio University  
Athens, OH 45701, USA

<sup>b</sup>TOTAL E&P  
CSTJF, Avenue Larribau  
F-64018 Pau  
France

<sup>c</sup>TOTAL RC  
TRTG - TOTAL Research & Technology Gonfreville  
BP 27 76 700 Harfleur - FRANCE

## ABSTRACT

Long-distance transmission of oil is usually carried out in large-diameter steel pipelines; water present therein may cause severe internal corrosion. An effective method of mitigating such corrosion is to inject organic corrosion inhibitors (CIs). Their surface adsorption, *via* heteroatom functionalities, can markedly enhance the corrosion resistance of metals. In this study, three CI model compounds with the same alkyl tail length ( $-C_{14}H_{29}$ ), specifically benzyl-dimethyl-tetradecyl-ammonium (BDTA), tetradecyltetrahydropyrimidinium (TTHP) and tetradecylphosphate ester (TPE) were synthesized, their purities being determined using nuclear magnetic resonance spectroscopy (NMR). The critical micelle concentrations (CMCs) of each compound were measured using surface tensiometry (Du Noüy ring) and fluorescence spectroscopy techniques, and differences were found between these indirect and direct methods. In addition, linear polarization resistance was used to determine inhibition efficiencies (IEs) for carbon steel immersed in a NaCl electrolyte saturated with  $CO_2$ . CI surface saturation concentrations, with maximum IEs, were compared with the determined CMCs. Excellent IEs were observed at concentrations of TTHP and TPE significantly less than their CMCs. These results imply that there is no direct link between CMC and corrosion efficiency and that the selection of the appropriate CI

concentration for an industrial application should not be based solely on CMC. Further work is ongoing to confirm this absence of correlation at higher temperature ( $T > 30^{\circ}\text{C}$ ) and different water chemistry.

Keywords: corrosion inhibitors, critical micelle concentrations, inhibition efficiency, surface saturation concentration

## INTRODUCTION

In the oil and gas industry, long-distance transportation of petroleum and related products is usually carried out in large-diameter carbon steel pipelines. Water present with the oil, along with corrosive species such as  $\text{CO}_2$ ,  $\text{H}_2\text{S}$  and organic acids, causes severe corrosion of the inner pipe walls.<sup>1</sup> An effective method of controlling corrosion is to continuously inject corrosion inhibitors into pipelines conveying oil-water mixtures. As corrosion occurs on water wetted metal surfaces, corrosion inhibitor (CI) molecules form protective films which reduce electrochemical reaction rates at the water-metal interface<sup>2</sup>, thereby protecting carbon steel pipes against  $\text{CO}_2$  ("sweet") corrosion and  $\text{H}_2\text{S}$  ("sour") corrosion.

Most commercial CIs are a complex mixture of several compounds that contain surfactant-type active ingredients, such as imidazoline, amine, phosphate ester, and quaternary ammonium derivatives<sup>3</sup>. Adsorption of organic molecules on surfaces through heteroatom functionalities, containing nitrogen, oxygen, sulfur and/or phosphorus, can markedly change the corrosion resistance properties of metals. Such molecules have a strong tendency to adsorb onto the steel surface and form self-assembled structures<sup>4,5</sup>. Surfactant-type organic inhibitors are, in some cases, applied based on their critical micelle concentration (CMC) values. However, recent work indicate that using CMC values as a measurement for injection of inhibitors might not be considered as a reliable factor<sup>6</sup>. CMC is an important characteristic of a surfactant. It is defined as the concentration of surfactants above which micelles form and all additional surfactant molecules added to the system aggregate as micelles<sup>7</sup>. As shown in Figure 1, below the CMC, the surfactant molecules will partition between the volume of the liquid and the gas-liquid interface with some CI molecules dispersed in the aqueous phase. Above the CMC, the concentration at the gas-liquid interface will not change anymore: any added surfactant molecule will tend to participate in the formation of micelles.

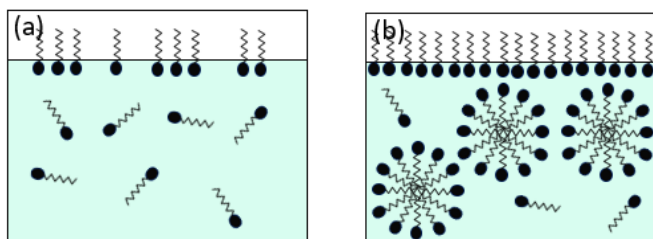


**Figure 1: Scenarios for different concentrations of the inhibitor in solution: (a) Below CMC; (b) Above CMC**

According to previous studies<sup>8-10</sup>, when the metal exhibits a maximum reduction of corrosion rate, its surface is considered to have reached a state of maximum coverage by inhibitor molecules; increasing the concentration of inhibitor in solution would not lead to an increase in surface coverage and the inhibited corrosion rate would remain constant. Hypothetically, this scenario can be said to also correspond to a situation where the inhibitor concentration reaches CMC, the inhibitor molecules cannot

continue to accumulate at interfaces and instead start forming micelles. Coincidentally, it is common to observe a sharp decrease in corrosion rate with the addition of CI but only to a certain concentration, above which no change in IE can be noticed. This threshold concentration, labeled surface saturation concentration and corresponding to a condition of maximum IE<sup>11</sup> have been often associated with CMC. Consequently, CMC has been used as an important parameter in determining corrosion inhibitor application concentrations and efficiencies. However, recent studies within our laboratory indicate that there is no direct link between CMC and surface coverage, and by extension corrosion inhibition efficiency<sup>6</sup>.

This paper reports the synthesis of three CI model compounds with the same alkyl tail length (-C<sub>14</sub>H<sub>29</sub>), namely benzyldimethyltetradecylammonium (BDTA), tetradecyltetrahydropyrimidinium (TTHP) and tetradecylphosphate ester (TPE), their purities being determined using nuclear magnetic resonance spectroscopy (NMR). The critical micelle concentrations (CMCs) of each compound were measured at 25°C using surface tensiometry (Du Noüy ring) and fluorescence spectroscopy (FS) techniques. Linear polarization resistance (LPR) was used to determine inhibition efficiencies (IEs) for carbon steel immersed in a NaCl electrolyte saturated with CO<sub>2</sub>. CI surface saturation concentrations, with maximum IE, were compared with the determined CMCs.

## EXPERIMENTAL METHODOLOGY

### Synthesis of Corrosion Inhibitor Model Compounds

#### Synthesis of benzyldimethyltetradecylammonium (BDTA)

The synthesis reaction for benzyldimethyltetradecylammonium (BDTA) bromide is as depicted in Figure 2. In this synthesis, acetonitrile (CH<sub>3</sub>CN) was chosen as the solvent as it was reported to achieve high amine quaternization rates<sup>12, 13</sup>.

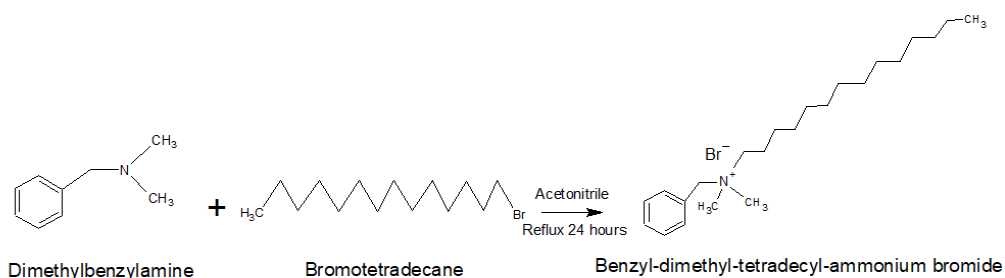


**Figure 2: The reaction for the model compounds BDTA utilized as a corrosion inhibitor**

The following presents the general procedure used for synthesizing the corrosion inhibitor model compound BDTA:

- (a) 13.52g (0.100 moles) of dimethylbenzylamine is added directly into a 2-necked 250mL round-bottomed flask (24/29 joints).
- (b) Acetonitrile solvent (100 mL) is then added, along with a few boiling chips.

- (c) A condenser and an addition funnel containing 27.73 g 1-bromotetradecane (also equivalent to 0.100 moles) are placed in each joint.
- (d) The round-bottom flask is then heated to the reflux temperature (82 °C) by an appropriately sized heating mantle connected to a Variac.
- (e) A flow of water runs through the condenser to ensure the reaction mixture (acetonitrile/amine mixture) is heated to the reflux temperature of ca. 82 °C.
- (f) The 1-bromotetradecane is then added dropwise from the addition funnel.
- (g) Reflux is maintained for a further 24 hours, then the reaction mixture is cooled to room temperature.
- (h) After the quaternization reaction is completed, the solvent is removed from the system by rotary evaporation.

### Synthesis of 1-tetradecyl-1,4,5,6-tetrahydropyrimidinium (TTHP)

The synthesis reaction is as depicted in Figure 3. In this reaction, a hydrogen ion ( $H^+$ ) resides on the more basic N atom; the N involved in the double bond. This N is more basic because a more stable (resonance stabilized) cation forms after protonation. However, it does not matter which of the two N's in 1,4,5,6-tetrahydropyrimidine is alkylated. In both cases, the same product forms. The final product is the one in which the positive charge is delocalized between the two nitrogen atoms. The real structure (resonance hybrid) is somewhere between the structures of the two resonance structures drawn in the below reaction scheme.

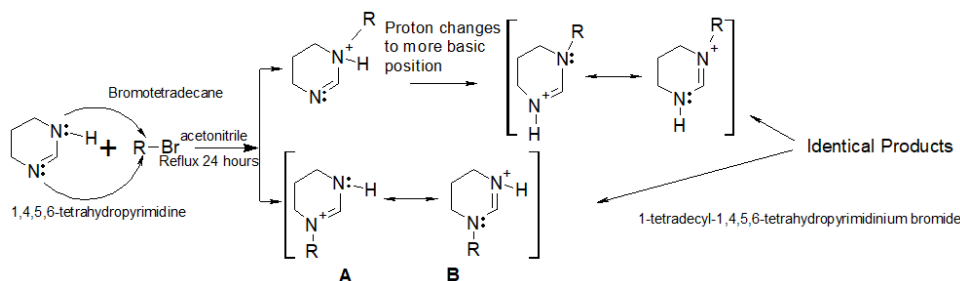


**Figure 3: The reaction for the synthesis of the TTHP model compound.**

The following is the procedure for the synthesis of 1-tetradecyl-1,4,5,6-tetrahydropyrimidinium, this is the same as that used in the synthesis of BDTA with tetrahydropyrimidine replacing dimethylbenzylamine:

- (i) 4.85 g (0.0576 moles) of 1,4,5,6-tetrahydropyrimidine is weighed directly into a 2-necked 250mL round-bottomed flask (24/29 joints).
- (j) Acetonitrile (100 mL) is added.
- (k) The round-bottom flask is placed in an appropriately sized heating mantle, four boiling stones being put into the flask to make sure there are plenty of nucleation sites for bubbles to form and prevent reaction mixture “bumping”.
- (l) The condenser and addition funnel containing 15.98 g (0.0576 moles) of 1-bromotetradecane are placed in each joint.

- (m) Cooling water is run through the condenser. The heating mantle, connected to a Variac, is switched on and set to ensure the reaction mixture (acetonitrile/pyrimidine mixture) is heated to the reflux temperature of ca. 82 °C.
- (n) The 1-bromotetradecane is then added dropwise to the reaction mixture, as shown in Figure 4 (a).
- (o) Reflux is maintained for a further 24 hours then the reaction mixture is cooled to room temperature.
- (p) The acetonitrile is removed by rotary evaporation (Figure 4 (b)). The temperature is increased to 95 °C, under vacuum, to drive off any residual volatile species.

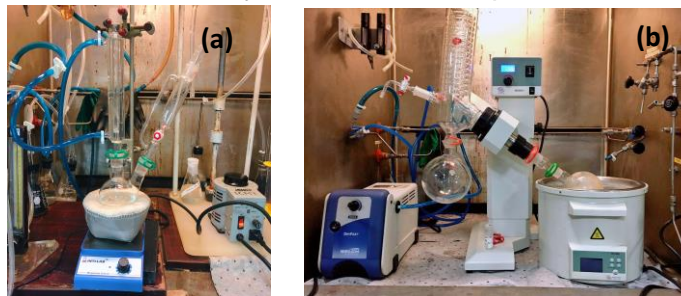


**Figure 4: (a) Reflux system for amine alkylation. (b) Recovery of products by rotary evaporation.**

#### Synthesis of Tetradecyl Phosphate Ester (TPE)

- *First step: Esterification*

The purpose of this step is to obtain a crude product, which may contain monoester, diester,  $\text{H}_3\text{PO}_4$ , and inorganic phosphates. The reaction is shown in Figure 5, where ROH is 1-tetradecanol ( $\text{C}_{14}\text{H}_{29}\text{OH}$ ). Note the reaction has no solvent.

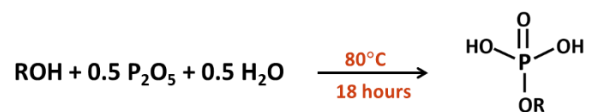


**Figure 5: Reaction for esterification**

- *Second step: Liquid-liquid extraction.*

The purpose of this step is to remove  $\text{H}_3\text{PO}_4$  and inorganic phosphates.

- *Third step: Rotary evaporation.*

The purpose of this step is to remove diethyl ether introduced by the second step as a solvent.

The following are the procedures for the synthesis of tetradecyl phosphate ester.

- *First step: Esterification.*
  - a) 42.8 g (0.2 moles) of solid 1-tetradecanol is weighed directly into a 3-necked 250mL round-bottomed flask.
  - b) 14.1g (0.1 moles) phosphorus pentoxide is added and mixed with the 1-tetradecanol.
  - c) Flask is set in a heating mantle.
  - d) Condenser, thermometer and addition funnel are placed in each joint.

- e) Water is run through the condenser and the reaction mixture is heated to ca. 80 °C, then held at that temperature for 6 hours.
  - f) 1.80 g (0.1 moles) of distilled water is placed in the addition funnel and is added dropwise to the reaction mixture.
  - g) The reaction is continued for a further 12 hours.
  - h) The product resembles a dark, oily liquid, which yields a waxy solid upon cooling.
- *Second step: Liquid-liquid extraction.*
    - a) This crude product is treated by liquid-liquid extraction using distilled water and diethyl ether to remove the phosphoric acid, and any inorganic phosphates, using an established procedure<sup>14</sup>.
    - b) Ether layers are drained using a separating funnel, placed in a 500mL single necked flask.
  - *Third step: Rotary evaporation.*
    - a) The ether is removed by rotary evaporation (Figure 4 (b)). The temperature is increased to 95 °C, under vacuum, to drive off any residual water.
    - b) The product is an oily liquid which, on cooling, yields a waxy solid; yield ca. 70%.

## Critical Micelle Concentration Measurements

### Determination of CMC using Surface Tension Measurement

The traditional measurement of surface tension is the Du Noüy ring method. Maximum pulling force on a ring by the surface is measured<sup>15</sup>. As described by Moradighadi, *et al*, the procedure for CMC measurements of the inhibitor model compounds was initiated by preparing NaCl solutions with different Cl concentrations using series dilution<sup>6</sup>. Before the measurement, the ring was cleaned with acetone and deionized water and then placed above the flame for a few seconds. Then, a Krüss K20 tensiometer was used to measure the surface tension of the solution at least twice. The procedure was typically stopped when the same/similar surface tension measurements occurred twice<sup>6</sup>.

### Determination of CMC using Fluorescence Spectroscopy

Fluorescence spectroscopy (FS) is a method used to exploit the fluorescence properties of a sample to determine concentrations of an analyte in solution. In fluorescence spectroscopy, a light with a specific wavelength is passed through the sample solution, which in turn emits fluorescence towards a filter and into a detector for measurement of the fluorescence emission intensity. The liquid soluble dye Nile Red<sup>16</sup> was used as the fluorescence probe in this study, since it demonstrated enhanced fluorescence in a hydrophobic environment, such as when micelles began to form. Fluorescence spectroscopy measurements were taken using a Fluorolog 3-FLC 21\* spectrofluorometer (Horiba Instruments, Edison, NJ). Nile Red (Molecular Probes and Acros) was used as the fluorophore probe. Dimethyl sulfoxide (DMSO, Fisher Scientific) was used as a non-polar solvent for the Nile Red powder. All the measurements were performed at least twice to confirm the accuracy of the results.

## Electrochemical Measurements

A three-electrode setup (Figure 6) was used to perform electrochemical experiments, with a C1018 rotating cylinder electrode (RCE) as a working electrode, a platinum-coated titanium mesh counter

---

\* Trade name

electrode, and an Ag/AgCl (KCl saturated) reference electrode. Before each experiment, the RCE was sequentially polished with 240, 400 and 600 grit silicon carbide abrasive papers, cleaned with isopropanol in an ultrasonic bath, and air-dried. The solution was deoxygenated for 2 hours by sparging with CO<sub>2</sub> before the introduction of the working electrode. After the RCE was inserted into the glass cell, a 20-minute pre-corrosion test was conducted (Figure 6) to determine whether the initial corrosion rate (CR) was close to the blank test and to ensure no contamination from the previous test. To minimize the noise in electrochemical measurements caused by CO<sub>2</sub> sparging, the sparge tube was retracted into the headspace during data acquisition. The solution was purged with CO<sub>2</sub> throughout the test to prevent air ingress and to saturate the test solution with CO<sub>2</sub>. The pH was adjusted by adding deoxygenated hydrochloric acid or sodium bicarbonate solution during each experiment.

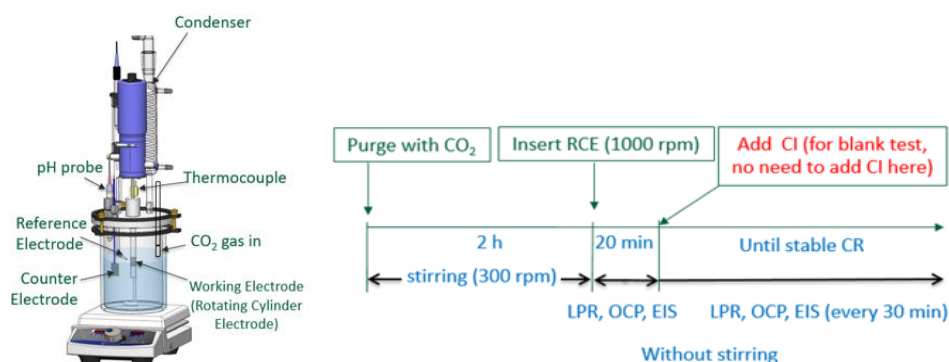


**Figure 6: Three-electrode setup and procedure used for corrosion experiments<sup>†</sup>.**

The corrosion rate was assessed by measuring linear polarization resistance (LPR) with a scan range from -5 mV to +5 mV *versus* OCP, a scan rate of 0.125 mV/s and a B value of 26 mV. The B value for these experiments was taken from previous research conducted on mild steel in a CO<sub>2</sub> environment<sup>17</sup> and was used in the analysis of all the experimental data reported herein. TPE and TTHP were evaluated in the experimental conditions shown in Table 1. Additional results obtained for BDTA by Moradighadi<sup>6</sup> are also shown for comparison purposes, although the experiments were performed in slightly different conditions: API 5L X65 carbon steel, 1 wt.% NaCl, 0.96 bar CO<sub>2</sub>, pH 4, 30 °C.

**Table 1**

**Experimental matrix for electrochemical experiments**

Description	Parameters
Working solution	50 g/L NaCl
Material	Carbon steel UNS G10180 (C1018)
Sparge gas	CO <sub>2</sub>
Temperature	25°C
pH	4.5
Cl model compound	1-tetradecyl-1,4,5,6-tetrahydropyrimidinium bromide (TTHP) and tetradecyl phosphate ester (TPE)
RCE velocity	1000 rpm

<sup>†</sup> Image courtesy of Cody Shafer, ICMT, Ohio University.

## RESULTS AND DISCUSSION

### Analysis of Products by NMR

#### Benzyl-dimethyl-tetradecyl-ammonium (BDTA)

The corrosion inhibitor BDTA was synthesized as described above then characterized. Proton nuclear magnetic resonance ( $^1\text{H-NMR}$ ) is the application of nuclear magnetic resonance in NMR spectroscopy with respect to hydrogen-1 nuclei within the molecules of a substance<sup>18</sup>. It can be used to determine the chemical structure of a synthesized compound and assessing its purity<sup>19</sup>. Any residual  $\text{CHCl}_3$  in the NMR solvent used (deuteriochloroform) produces a peak at  $\delta=7.25\text{ppm}$ . By using a web-based NMR tool<sup>20</sup>, the peak positions for  $^1\text{H-NMR}$  spectra were simulated. Figure 7 shows the NMR spectrum for the synthesized model compound BDTA. The numbers of hydrogen atoms of each molecular position (from a to q) are pointed out in each peak. The spectrum indicates the product is free of acetonitrile (solvent) as well as 1-bromotetradecane and dimethylbenzylamine reactant. It showed an excellent agreement with the expected structure based upon the simulated spectrum. Moreover, peaks unrelated to the structure were numerically integrated to determine the level of negligible impurities (product ca. 99%+ purity).

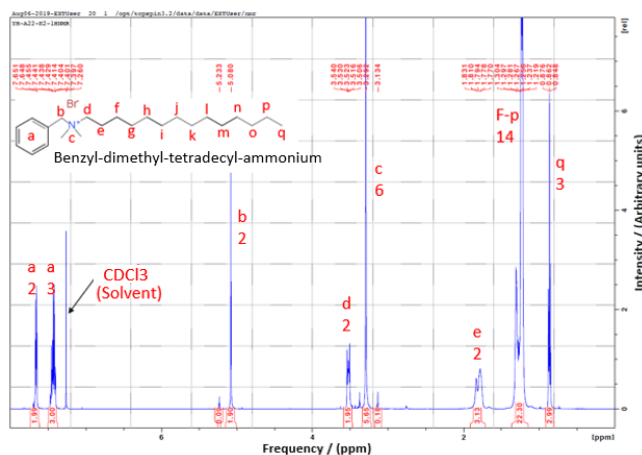


**Figure 7:  $^1\text{H-NMR}$  spectrum of the synthesized corrosion inhibitor model compound BDTA.**

#### 1-Tetradecyl-1,4,5,6-tetrahydropyrimidinium (TTHP)

Figure 8 shows the  $^1\text{H NMR}$  spectrum for the synthesized model compound TTHP. The spectrum indicates the product is free of acetonitrile (solvent) as well as 1-bromotetradecane and tetrahydropyrimidine reactants. It showed excellent agreement with the expected structure based upon the simulated NMR spectrum. Moreover, peaks unrelated to the structure were numerically integrated to determine the level of negligible impurities (product ca. 99%+ purity).

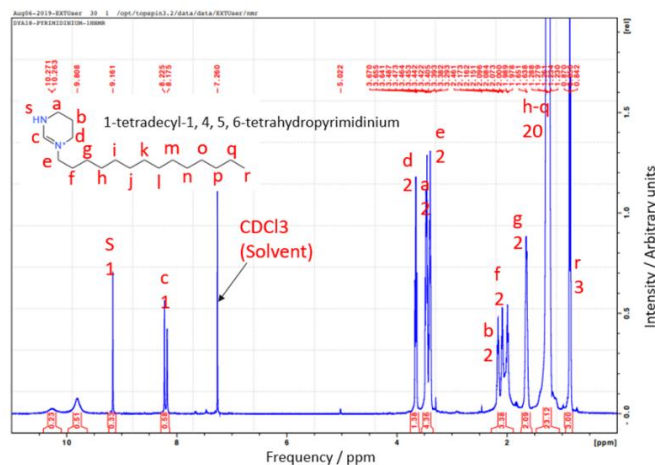


**Figure 8:  $^1\text{H}$ -NMR spectrum of the synthesized corrosion inhibitor model compound TTHP.**

### Tetradecyl Phosphate Ester (TPE)

Again, using a web-based NMR tool<sup>20</sup>, the peak positions in the  $^1\text{H}$  NMR spectra were simulated for 1-tetradecanol, monoester, and diester. Comparing the  $^1\text{H}$  NMR spectra of the crude products with that simulated, the result indicates that there are monoester and/or diester molecules in the crude products. There is essentially no 1-tetradecanol in the crude products, indicating it has reacted totally in the esterification step.

The detected  $^{31}\text{P}$  NMR spectrum of the crude product is shown in Figure 9. By comparing with standard  $^{31}\text{P}$  NMR spectra, all these peaks have been identified as monoester, diester, and  $\text{H}_3\text{PO}_4$ /inorganic phosphates. By integrating the corresponding peak area, the ratio of these three categories is approximately 3:1:1.

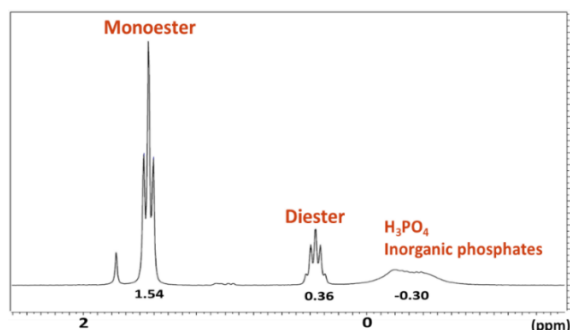


**Figure 9: Detected  $^{31}\text{P}$  NMR spectra of crude products.**

The detected  $^{31}\text{P}$  NMR spectrum of final purified products, after liquid-liquid extraction, is shown in Figure 10. Comparing the detected  $^{31}\text{P}$  NMR spectra of crude product and final product, the peak for  $\text{H}_3\text{PO}_4$  and inorganic phosphates has disappeared, which indicates that  $\text{H}_3\text{PO}_4$  and inorganic phosphates have been removed by the second and third steps. By integrating the peak area, the final product consists of 73.5% monoester and 26.5% diester.

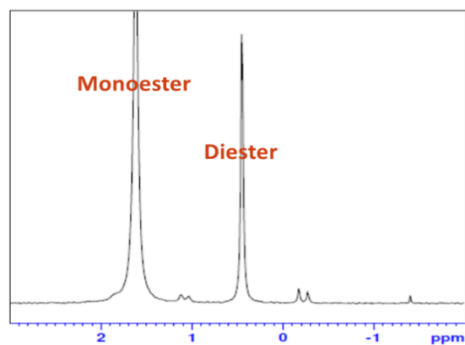


Figure 10: Detected  $^{31}\text{P}$  NMR spectra of purified product.

## Critical Micelle Concentration Measurements

### Determination of CMC using Surface Tension Measurement

Figure 11 shows surface tension measurements of model inhibitor compound TTHP and TPE. With the increase in inhibitor concentration in an aqueous solution, the solution/air interfacial tension decreases until it approaches a constant value at around 30 mN/m (*i.e.*, its variation is within the measurement error), assumed to correspond to the onset of micelle formation in the bulk and termed the CMC. For model inhibitor compound TTHP (Figure 11(a)), the intersection of the two lines for the test is  $35 \pm 5$  ppm<sub>w</sub>. For model inhibitor compound TPE (Figure 11(b)), the intersection of the two lines for the test is  $25 \pm 5$  ppm<sub>w</sub>.

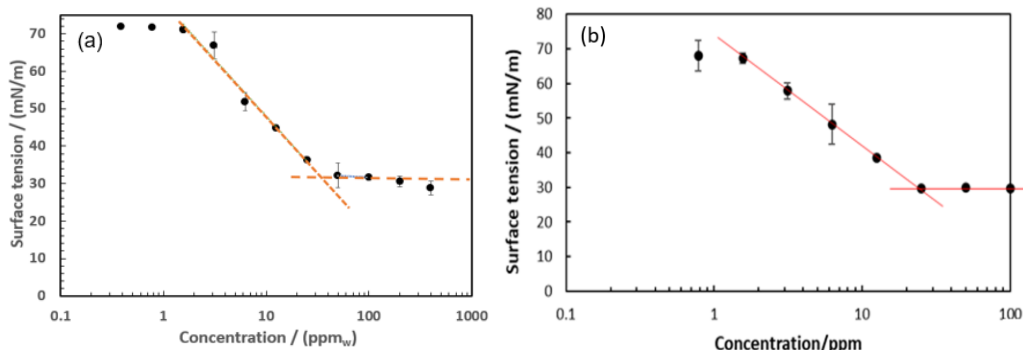
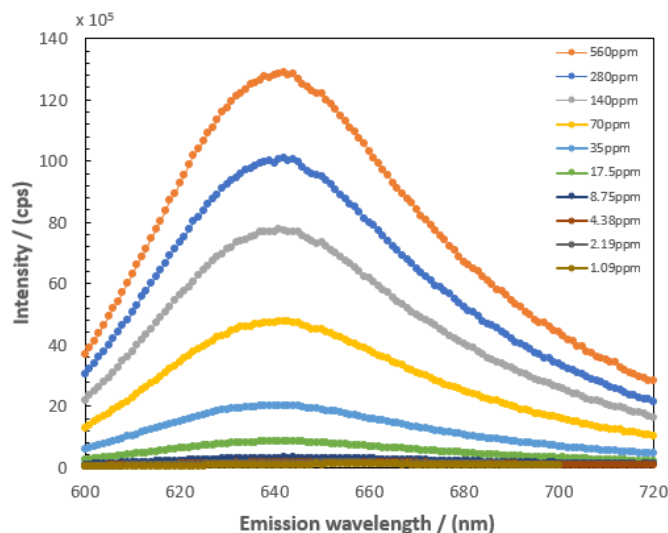


Figure 11: Surface tension measurements of model inhibitor compound. (a) TTHP (b) TPE.

### Determination of CMC using Fluorescence Spectroscopy

The fluorescence emission intensities for TTHP with different concentrations in 50 g/L NaCl solution are shown in Figure 12. From the graph, there was an enhanced increase in emission intensity at 35 ppm<sub>w</sub> of TTHP inhibitor solution, which indicates the formation of micelles in the bulk solution. The CMC of TTHP was determined within the range of 17.5~35 ppm<sub>w</sub> using fluorescence spectroscopy.



**Figure 12: Fluorescence spectroscopy of TTHP in 50 g/L NaCl solution.**

The emission intensity with a series of TPE concentrations is shown in Figure 13. The emission intensity increased with TPE concentration. When the concentration was increased to 100 ppm<sub>w</sub>, a significant increase in emission intensity was observed, which implies the formation of micelles in the bulk solution. However, no clear increase in emission intensity was detected with the addition of 50 ppm<sub>w</sub>. According to the results, TPE micelles started to form at a concentration of around 100 ppm<sub>w</sub>. Consequently, the CMC value for TPE in 5 wt% NaCl solution was determined within the range of 50~100 ppm<sub>w</sub> using fluorescence spectroscopy.

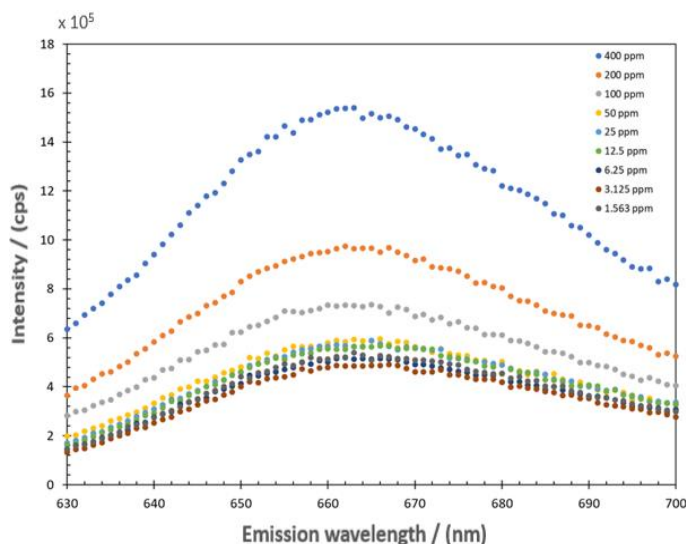


**Figure 13: Fluorescence spectroscopy of TPE in 50 g/L NaCl solution.**

Moradighadi, *et al.* studied CMC measurements of BDTA corrosion inhibitor model compounds. The result shows that CMC of BDTA in 1 wt% NaCl is  $50 \pm 5$  ppm<sub>w</sub> using both surface tension measurement<sup>6</sup> and fluorescence spectroscopy<sup>21</sup>. From the above results, the CMC of BDTA and TTHP were determined to be the same using both Du Noüy Ring surface tension measurement and fluorescence spectroscopy.

However, for TPE, there is a clear discrepancy between the CMC value measured by the fluorescence spectroscopy method (between 50 and 100 ppm<sub>w</sub>) and the CMC value measured using the surface tension method (25 ppm<sub>w</sub>). The surface tension method indirectly evaluates the micelle formation in a bulk solution *via* measurement at the interface between solution and air. However, the fluorescence spectroscopy, with respect to the determination of the CMC, is more direct than the Du Nouy method since it characterizes concentration and the nature of inhibitor molecules in a bulk solution, whether they micellized or not. In this view, fluorescence spectroscopy is thought to be more accurate to detect the formation of micelles.

### Correlation Between CMC and Inhibition Efficiency

The correlation between CMC and inhibition efficiency can be achieved by comparing the corrosion inhibition parameters for the same inhibitor. As proposed by Hackerman, *et al.*, the saturation of the metal surface by adsorbed corrosion inhibitor means that the corrosion inhibitor will continue to adsorb on the metal surface until the surface is saturated with the inhibitor<sup>22</sup>. Any further addition of the inhibitor to the bulk solution does not result in further adsorption and a further decrease in the corrosion rate. The amount of the inhibitor added is called the surface saturation concentration<sup>22</sup>. The surface saturation concentration is the minimum concentration that yields the maximum efficiency of a corrosion inhibitor.

Figure 14 shows the corrosion rate of C1018 steel in the absence of inhibitor and with various concentrations of TTHP. The C1018 RCE was immersed in 50 g/L NaCl electrolyte at 25°C. In the absence of inhibitor, the corrosion rate was  $2.01 \pm 0.13$  mm/yr. In the presence of TTHP, the corrosion rate gradually decreased with increasing inhibitor concentration from 0.25 to 8.75 ppm<sub>w</sub>. When the CI concentration is above 8.75 ppm<sub>w</sub>, the corrosion rate remained low at  $0.11 \pm 0.02$  mm/yr and relatively insensitive to the inhibitor concentration. The surface saturation concentration of TTHP in 50 g/L NaCl was determined to be within the range of 1 to 8.75 ppm<sub>w</sub>.

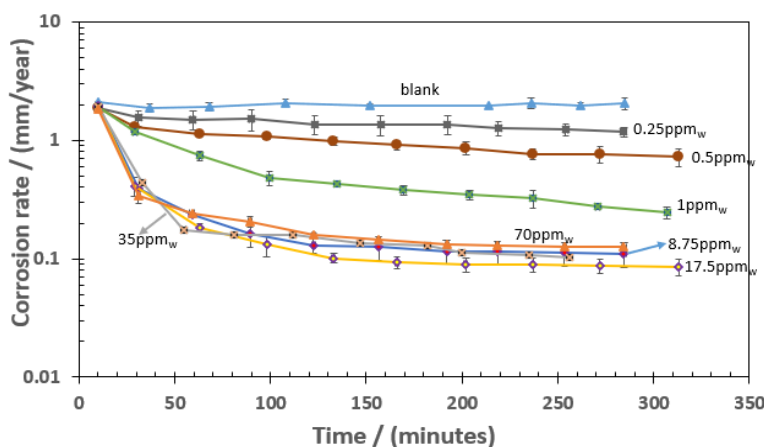


**Figure 14: LPR measured corrosion rates of the C1018 carbon steel immersed in 50 g/L NaCl solution in the presence and absence of TTHP at 25°C as a function of time.**

Figure 15 shows the corrosion rate of C1018 steel in the absence of inhibitor and with various concentrations of TPE. In the absence of an inhibitor, the corrosion rate was  $2.00 \pm 0.15$  mm/yr. In the presence of TPE, the corrosion rate gradually decreased with increasing inhibitor concentration from 0.5 to 3 ppm<sub>w</sub>. When the CI concentration is above 3 ppm<sub>w</sub>, the corrosion rate remained low at  $0.08 \pm 0.03$

mm/yr and relatively insensitive to the inhibitor concentration. The surface saturation concentration of TPE in 50 g/L NaCl was determined to be within the range of 2 to 3 ppm<sub>w</sub>

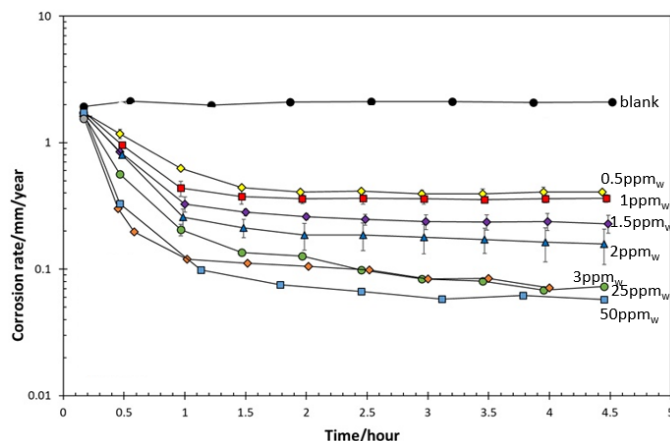


**Figure 15: LPR measured corrosion rates of the C1018 carbon steel immersed in 50 g/L NaCl solution in the presence and absence of TPE at 25°C as a function of time.**

The corrosion mitigation efficiency was calculated when the corrosion rate did not significantly change over time (less than  $\pm 0.01$  mm/year between measurements)<sup>11</sup>. Equation (1) was used<sup>23</sup> to calculate the corrosion mitigation efficiency ( $\epsilon$ ):

$$\epsilon = 1 - \frac{(CR)_\theta}{CR} \quad (1)$$

where  $(CR)_\theta$  was the corrosion rate of the system with corrosion inhibitor and CR represented the corrosion rate of the same system without the inhibitor present. Table 2 summarizes the above results of different corrosion inhibitor model compounds.

**Table 2**  
**Parameters of corrosion inhibitor model compounds.**

Type of inhibitor	CMC value by Surface Tension Measurements (ST) and Fluorescence Spectroscopy (FS) (ppm <sub>w</sub> )		Surface Saturation Concentration (ppm <sub>w</sub> )	Steady State Inhibited Corrosion Rate (mm/year)	Inhibition Efficiency
	ST	FS			
BDTA	50 ± 5 <sup>6</sup>	50 ± 1 <sup>21</sup>	25~50 <sup>6</sup>	0.22 ± 0.04 <sup>6</sup>	93% <sup>6</sup>
TTHP	35 ± 5	17.5~35	1~8.75	0.11 ± 0.02	95%
TPE	25 ± 5	50~100	2~3	0.08 ± 0.03	95%

Moradighadi, *et al.* conducted LPR corrosion rate measurements in the presence of BDTA at different concentrations<sup>6</sup>. The surface saturation concentration in 1 wt% NaCl, pH 4, 30 °C was determined to be within the range of 25 to 50 ppm<sub>w</sub> based on the maximum efficiency of the tested inhibitor. Interestingly, BDTA has similar values for CMC and surface saturation concentration, however, the corrosion inhibition efficiencies for both TTHP and TPE inhibitors do not correspond with their CMC value. The surface

tension and fluorescence spectroscopy measurements used for most CMC evaluations are conducted at the air/solution interface or in bulk solution, which may not necessarily have a direct relationship to the inhibitor coverage at the metal/solution interface<sup>21</sup>. Consequently, these results indicate that there is no direct link between CMC and surface coverage, and by extension to corrosion inhibition efficiency. The optimal inhibitor concentration used in a pipeline should be chosen based on the actual corrosion inhibition efficiency, instead of the CMC. CMC alone is not enough to the statute on the efficiency of a given corrosion inhibitor. Furthermore, the maximum corrosion inhibition efficiency is 95%, which means that the corrosion cannot become fully inhibited/stopped at the maximum inhibition efficiency; corrosion will always happen, albeit mitigated. In practice, this residual corrosion rate is actually of great interest to operators.

## CONCLUSIONS

- Three CI model compounds with the same alkyl tail length (-C<sub>14</sub>H<sub>29</sub>), specifically benzyldimethyltetradecylammonium (BDTA), tetradecyltetrahydropyrimidinium (TTHP) and tetradecylphosphate ester (TPE) were synthesized. Their purities being determined using nuclear magnetic resonance spectroscopy (NMR)
- CMC values were obtained by surface tension measurements and fluorescence spectroscopy, differences being found between these indirect and direct methods. The fluorescence spectroscopy, with respect to the determination of the CMC, seems to be a more direct measurement technique than the Du Nouy method.
- The correlation between CMC and inhibition efficiency was achieved by comparing the corrosion inhibition parameters for the same inhibitor. Results indicate that there is no direct link between CMC and surface coverage, and by extension to corrosion inhibition efficiency. CMC alone is consequently not an accurate indicator to assess the performance or the needed dosage of a given CI – in some cases, it can be completely misleading.

## ACKNOWLEDGMENTS

This project has been supported by TOTAL transversal R&D project (MANA Project). The authors would like to thank TOTAL for their financial support and valuable discussions. Prof. Klaus Himmeldirk from Ohio University is thanked for the discussion of the synthesis of TTHP and supplying Figure 3.

## REFERENCES

1. M. B. Kermani and D. Harrop, "The impact of corrosion on the oil and gas industry," *SPE Prod. Facil.*, vol. 11, no. 3, pp. 186–190, 1996.
2. Y. Xiong, B. Brown, B. Kinsella, S. Nešić, and A. Pailleret, "Atomic force microscopy study of the adsorption of surfactant corrosion inhibitor films," *Corrosion*, vol. 70, no. 3, pp. 247–260, 2014.
3. Y. Duda, R. Govea-Rueda, M. Galicia, H. I. Beltraén, and L. S. Zamudio-Rivera, "Corrosion inhibitors: Design, performance, and computer simulations," *J. Phys. Chem. B*, vol. 109, no. 47, pp. 22674–22684, 2005.
4. V. S. Sastri, *Green Corrosion Inhibitors: Theory and Practice*, 2nd ed. Hoboken, NJ: John Wiley & Sons, 2011.
5. S. Sharma, X. Ko, Y. Kurapati, H. Singh, and S. Nešić, "Adsorption behavior of organic

corrosion inhibitors on metal surfaces—some new insights from molecular simulations,” *Corrosion*, vol. 75, no. 1, pp. 90–105, 2019.

6. N. Moradighadi, S. Lewis, J. M. Domínguez Olivo, D. Young, B. Brown, and S. Nestic, “Effect of alkyl tail length on CMC and mitigation efficiency using model quaternary ammonium corrosion inhibitors,” in *Corrosion/19*, paper no. 13004 (Nashville, TN: NACE, 2019).
7. H. Sawai and L. E. Orgel, “Oligonucleotide Synthesis Catalyzed by the Zn<sup>2+</sup> Ion,” *Journal of the American Chemical Society*, vol. 97, no. 12. Blackwell Scientific Publications, Oxford, pp. 3532–3533, 1975.
8. M. A. Malik, M. A. Hashim, F. Nabi, S. A. AL-Thabaiti, and Z. Khan, “Anti-corrosion ability of surfactants: A review,” *International Journal of Electrochemical Science*, vol. 6, no. 6. pp. 1927–1948, 2011.
9. M. L. Free, “Understanding the effect of surfactant aggregation on corrosion inhibition of mild steel in acidic medium,” *Corros. Sci.*, vol. 44, no. 12, pp. 2865–2870, 2002.
10. L. El Achouri, I. M., Bensouda, Y., Gouttaya, H. M., Nciri, B., Perez, “Gemini surfactants of the Type 1,2-ethanediyl bis-(dimethylalkylammonium bromide),” *Tenside Surfactants Deterg.*, vol. 38, no. 4, pp. 208–215.
11. J. M. Domínguez Olivo, B. Brown, D. Young, and S. Nestic, “Electrochemical model of CO<sub>2</sub> corrosion in the presence of quaternary ammonium corrosion inhibitor model compounds,” in *Corrosion/19*, paper no. 13392 (Nashville, TN: NACE, 2019).
12. S. Patai, “Chemistry of the amino group,” in *Wiley-Interscience*, 1968, pp. 45–52.
13. H. Z. Sommer, H. I. Lipp, and L. L. Jackson, “Alkylation of amines. A general exhaustive alkylation method for the synthesis of quaternary ammonium compounds,” *J. Org. Chem.*, vol. 36, no. 6, pp. 824–828, 1971.
14. Y. Shi, Y. Zhao, G. Zhang, and Q. Dong, “Synthesis and properties of lauryl phosphate monoester,” *Tenside, Surfactants, Deterg.*, vol. 56, no. 3, pp. 244–251, 2019.
15. S. Ebnesajjad, *Handbook of Adhesives and Surface Preparation*. 2011.
16. P. Greenspan and S. D. Fowler, “Spectrofluorometric studies of the lipid probe, Nile red,” *J. Lipid Res.*, vol. 26, no. 7, pp. 781–789, 1985.
17. Z. Belarbi, F. Farel, M. Singer, and S. Nestic, “Role of amine in the mitigation of CO<sub>2</sub> TOP of the line corrosion,” *Corrosion*, vol. 2, no. 7274, pp. 1256–1270, 2016.
18. R. M. Silverstein, G. C. Bassler, and T. C. Morrill, *Spectrometric identification of organic compounds*, 5th ed. 1991.
19. Whittaker D., *Interpreting organic spectra*. Royal Society of Chemistry, 2007.
20. Nmrdb.org, “Tools for NMR spectroscopists.” <http://www.nmrdb.org/>.
21. N. Moradighadi, S. Lewis, J. M. Domínguez Olivo, D. Young, B. Brown, and S. Nestic. “Determining Critical Micelle Concentration of Organic Corrosion Inhibitors and the Role in Corrosion Mitigation.” *Corrosion*, in press.

22. T. Murakawa, S. Nagaura, and N. Hackerman, "Coverage of iron surface by organic compounds and anions in acid solutions," *Corros. Sci.*, vol. 7, no. 2, pp. 79–89, 1967.
23. S. Papavinasam, "Evaluation and selection of corrosion inhibitors," *Uhlig's Corros. Handb.*, pp. 1169–1178, 1999.